A Kirchhoff integral approach for decimetric radiowave propagation in urban areas

L. Pisani, F. Rapetti, C. Vittoli

Centro di Ricerca, Sviluppo e Studi Superiori in Sardegna (CRS4)
Via N. Sauro 10, 09123 Cagliari, Italy.

Abstract

We consider a three-dimensional approach based on the Kirchhoff's method in order to predict electromagnetic waves propagation in urban environments. In particular, we are interested here in the evaluation of the electromagnetic field on very large three-dimensional domains (typically with linear dimensions of the order of hundreds of meters) generated by a high frequency source (typically of the order of 1GHz which corresponds to a wavelength of about 30 centimeters). Some numerical tests and comparisons with experimental measurements have been done to validate this approach.

1 Introduction

Efficient planning of mobile communication systems is based on an accurate determination of the coverage region of the antenna. In urban environments, this can be quite complicated, since electromagnetic waves are absorbed, reflected, transmitted and diffracted by buildings. The subject of our research activity is the analysis and development of simulation tools to effectively predict the propagation of the electromagnetic waves and the antenna coverage in three-dimensional urban domains which have huge dimensions with respect to the wavelength.

Techniques used to solve this problem in a reasonably fast way include ray tracing (Ikegami *et al.*, 1991, Rossi *et al.*, 1992, Kürner *et al.*, 1993, Rizk *et al.*, 1994) and two-dimensional Transmission Line Matrix (TLM) (Luthi *et al.*, 1996). We propose a three-dimensional approach based on the Kirchhoff integral method. The presence of multiple reflections has led to implement Kirchhoff's method using an iterative procedure where each iteration corresponds to a reflection on a surface. In addition, a number of approximations have been introduced to limit the computational complexity.

This approach is validated through numerical comparisons with experimental measurements. Further results related to the convergence and time scaling of the method as well as its application to determine the antenna coverage in urban environments are presented and discussed.

2 The vector Kirchhoff integral relation

In this section we review the theoretical basis of the vector Kirchhoff integral relation (Jackson, 1975, pages 432-435).

Suppose that the vector field $\mathbf{E}$ has harmonic time dependence $e^{-i\omega t}$. When the field sources are outside the volume V, the field $\mathbf{E}$ satisfies the vector Helmholtz wave equation inside V,

$$(\nabla^2 + k^2)\mathbf{E}(\mathbf{x}) = 0 \tag{1}$$

where $k = \frac{\omega}{c}$ and c is the wave propagation velocity. By applying the divergence theorem

$$\oint_V \nabla dV = \oint_{S_V} \mathbf{n} d\sigma \tag{2}$$

it is easy to see that, when equation (1) is verified, the following relation is an identity:

$$\mathbf{E}(\mathbf{x}) = \oint_{S_V} [\mathbf{E}(\mathbf{n}' \cdot \nabla' \frac{e^{ikr}}{4\pi r}) - \frac{e^{ikr}}{4\pi r}(\mathbf{n}' \cdot \nabla')\mathbf{E}]\, dx' \tag{3}$$

In (3) $\mathbf{r} = \mathbf{x} - \mathbf{x}'$, the point $\mathbf{x}$ is inside the volume V bounded by the surface S_V and the unit normal $\mathbf{n}'$ is directed into the volume V.

Equation (3), which is known as the Kirchhoff integral, expresses the electric field $\mathbf{E}$ at a point $\mathbf{x}$ inside a

closed volume V in terms of the values of the field and its normal derivative on the boundary surface S_V. By using Maxwell equations, we can rewrite equation (3) in terms of the electric and magnetic fields $\mathbf{E}$ and $\mathbf{B}$:

$$\mathbf{E}(\mathbf{x}) = \frac{i}{4\pi} \oint_{S_V} \frac{e^{ikr}}{r} \left[\mathbf{k} \times (\mathbf{n}' \times \mathbf{E}) \left(1 + \frac{i}{k\,r}\right) + k(\mathbf{n}' \times \mathbf{B}) - \mathbf{k}(\mathbf{n}' \cdot \mathbf{E}) \left(1 + \frac{i}{k\,r}\right) \right] d\mathbf{x}' \quad (4)$$

For the Helmholtz equation (1) to be satisfied inside V, the medium contained in V must be homogeneous. Therefore, when we need to evaluate the electromagnetic scattering from objects which have a dielectric constant $\epsilon \neq \epsilon_0$, we can identify V with the free space between the scatterers. The boundary surface S_V of V is taken equal to $S \cup S_\infty$ where S is the surface of the scattering objects and S_∞ is the surface "at infinity". It can be proven (Jackson, 1975, pages 433-434) that the integral over S_∞ vanishes; so the integral in (4) can be computed only over S.

It is useful to specialize (4) to a scattering situation and to exhibit a formal expression for the scattering amplitude as an integral of the scattered fields over S. Since the scattering objects are supposed to be outside the volume V, equation (4) holds for the scattered fields $(\mathbf{E_s}, \mathbf{B_s})$, that is, the total fields $(\mathbf{E}, \mathbf{B})$ minus the incident fields $(\mathbf{E_i}, \mathbf{B_i})$ (i.e., the fields generated by active sources such as antennas). In equation (4) $\mathbf{E}(\mathbf{x})$ depends explicitly on the outgoing direction of $\mathbf{k}$. The dependence on the incident direction is implicit in the scattered fields $\mathbf{E}$ and $\mathbf{B}$.

3 Description of the model

The evaluation of the field $\mathbf{E}$ through equation (4), requires the knowledge of the fields $\mathbf{E_s}$ and $\mathbf{B_s}$ on the surface S.

3.1 A single scatterer

In the absence of knowledge about the correct fields $\mathbf{E}_s$ and $\mathbf{B}_s$ on the surface S, we must make some approximations.

First, we neglect the field transmitted through the building. This is equivalent to assuming that the building is an "opaque" object. This assumption is reasonable at the frequencies we are dealing with as the part of the wave energy which is not reflected from the surface, is largely dissipated inside the building. Because the wavelength is small with respect to the linear dimensions of the obstacle, the surface S of the building can be divided approximately into an illuminated region S_i and a shadowed one S_s. In the shadowed region the total field on the surface S_s is nearly zero (the object is opaque). We assume that there the scattered field on S_s is equal and opposite to the incident field. In addition, we suppose that the building's external walls are either flat or with a radius of curvature large with respect to the wavelength. As a result, in the illuminated region, Fresnel coefficients for reflection are used to evaluate the scattered field on S_i. This procedure can be summarized as follows:

s1) the incident fields $\mathbf{E}_i$ and $\mathbf{B}_i$ (generated by the antenna) are evaluated on the surface S of the scatterer;

s2) the scattered fields $\mathbf{E}_s$ and $\mathbf{B}_s$ on S are approximated as described above;

s3) the scattered fields throughout the space V are computed using the Kirchhoff integral method.

This method gives a good estimate of the scattered field around an opaque object. If the diffraction effects on the building wedges are negligible, we can simplify the above procedure by assuming a "Geometrical Optics" shadow for the incident field, i.e. by assuming that both the incident and scattered fields are equal to zero beside the obstacle. When we are dealing with a large number of scatterers, this approximation can allow a sensible reduction in the computational time, because it reduces the number of pair-interactions (only the pairs of scatterers that "see" each other interact). This aspect will be discussed in detail in section 4.1. Later on this paper, we will refer to the first procedure as the "general procedure" and to the second as the "GOS (Geometrical Optics Shadow) procedure".

3.2 More than one scatterer

When dealing with more than one building, the procedure for one scatterer can be extended using an iterative technique where each iteration corresponds to a reflection on a surface.

a: The incident field produced by all the sources is evaluated on each building surface S_n:

- at the first iteration, the only source is the antenna;
- starting from the second iteration, the sources of incident field are the antenna and all the surfaces which have been illuminated during the previous iteration. The second contribution is evaluated by using the Kirchhoff integral.

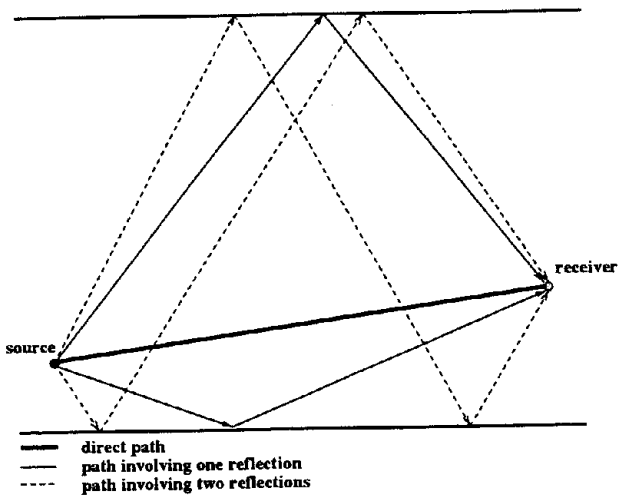

Figure 1: Example of source-receiver paths involving up to two reflections. These paths are accounted for by the method after two iterations

b: When the incident fields $\mathbf{E}_i$ and $\mathbf{B}_i$ are known at each point of the surface S_n, the scattered fields $\mathbf{E}_s$ and $\mathbf{B}_s$ on S_n are evaluated as described in section 3.1. At the frequencies considered, the diffraction fields are small with respect to the Geometrical Optics fields and they can be neglected if the intensity of incident radiation is low. Therefore, we have chosen to evaluate the scattered fields on S_n by using the "general procedure" when the source of the incident fields $\mathbf{E}_i$ and $\mathbf{B}_i$ is the antenna and the "GOS procedure" elsewhere. $\mathbf{E}_s$ and $\mathbf{B}_s$ will be used in the first step of the next iteration to compute the incident field on the other surfaces.

c: When the electromagnetic fields do not significantly change from one iteration to the next one, the procedure ends.

d: At the end of the iterative procedure, we know the electromagnetic fields on all the involved surfaces and we can use, once again, the Kirchhoff integral to evaluate the electromagnetic field throughout the domain V.

The above procedure is sketched in figure 1 in the case of two buildings and up to the second iteration. It is seen that, each iteration is equivalent to include new paths connecting the source to the receiver.
To analyze the convergence of the method, we consider the configuration described in figure 2. A plane wave of wavelength $\lambda = 6.28$ meters and wave vector $\mathbf{k} = (0.89, 0.42, -0.15)$, whose projection onto $z = 0$ is drawn in the picture, has been taken as the incident field. At each iteration, the field values are measured at points located at a height of 1.8 meters, along the axis shown in the figure.

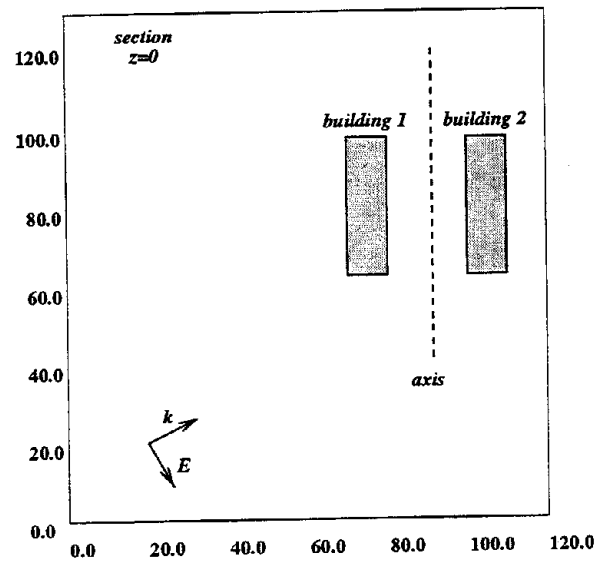

Figure 2: Geometry used to test convergence of the method. Receivers are located along the dashed line between the two buildings (all dimensions are given in meters)

At iteration n, the convergence of the method is checked through the following parameters:

$$\mathrm{er}^n_{E_i} = \max\left\{|E^n_i(k) - E^{n-1}_i(k)|, k = 1, N_r\right\}, \quad i = 1,3$$

$$\mathrm{er}^n_E = \max\left\{\mathrm{er}^n_{E_i},\ i = 1,3\right\}$$

where N_r is the number of receivers.
Figure 3 reports the values of er^n_E at each iteration. The lines refer to two different simulations where the buildings are considered either metallic or built with material of dielectric constant $\epsilon = 4$. In the second case, the convergence is faster because, at each iteration, part of the incident energy is absorbed by the external walls.
In figure 4 we report the values of two components of the electromagnetic field, computed in the case of metallic buildings. The convergence of the component E_y is much slower than that of the component E_x. This can be intuitively explained by noting that an y-directed electric field can be associated to an x-directed wave, which is reflected between the metallic walls as in a resonating cavity, while the x-directed electric field, related to an y-directed wave, is free to leave the system. So we expect that the y component will keep changing at each iteration (and further reflection) between the buildings (i.e. $65 < y < 100$) more than outside them, and this is confirmed by the results of the simulation shown in figure 4 (bottom).

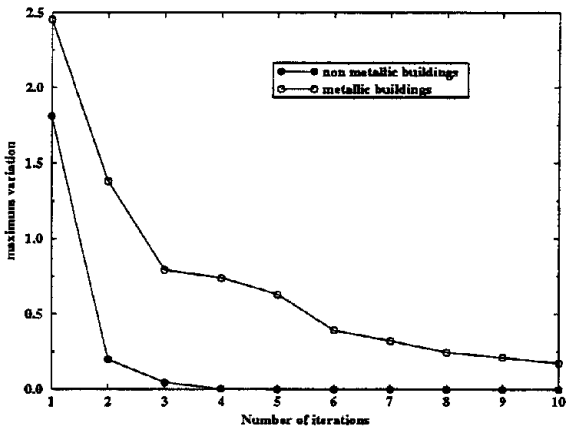

Figure 3: Convergence of the method. White dots refer to perfectly conducting surfaces. Black dots refer to dielectric surfaces ($\epsilon = 4$). The quantity "maximum variation", reported on y axis, is defined as $\mathrm{er}_E^n = \max\{\mathrm{er}_{E_i}^n,\ i = 1,3\}$, where $\mathrm{er}_{E_i}^n$ is $\mathrm{er}_{E_i}^n = \max\{|E_i^n(k) - E_i^{n-1}(k)|, k = 1, N_r\}$, $i = 1,3$ and N_r is the number of receivers

4 Computational aspects

In this section we present the main computational features of the model.

4.1 Scaling of the computer time with the dimension of the domain

The model described in section 3 requires, on each surface, the evaluation of the field scattered from the other surfaces. Thus, at first sight, the computational time grows as N^2 with N the number of surface elements and as D^4 with D the diameter of the domain. This behavior is even worse than the one shown by the methods which require the discretization of the whole space (D^3), but, as we will show, can be easily improved.

Consider the situation described in figure 5. S_2 is a region of the surface on which we need to compute the field scattered by a region S_1 of another surface; we can write

$$\mathbf{r} = \mathbf{r}_0 - \mathbf{x}' + \mathbf{x}''$$

and

$$r = \left[r_0^2 - 2\mathbf{r}_0 \cdot (\mathbf{x}' - \mathbf{x}'') + |\mathbf{x}' - \mathbf{x}''|^2\right]^{\frac{1}{2}}$$

When r is large compared with x' and x'', we can rewrite r using a suitable Taylor expansion:

$$r = r_0 - \frac{\mathbf{r}_0 \cdot (\mathbf{x}' - \mathbf{x}'')}{r_0} + T \qquad (5)$$

where

$$T = \frac{|\mathbf{x}' - \mathbf{x}''|^2}{2r_0} - \frac{[\mathbf{r}_0 \cdot (\mathbf{x}' - \mathbf{x}'')]^2}{2r_0^3} + \ldots \qquad (6)$$

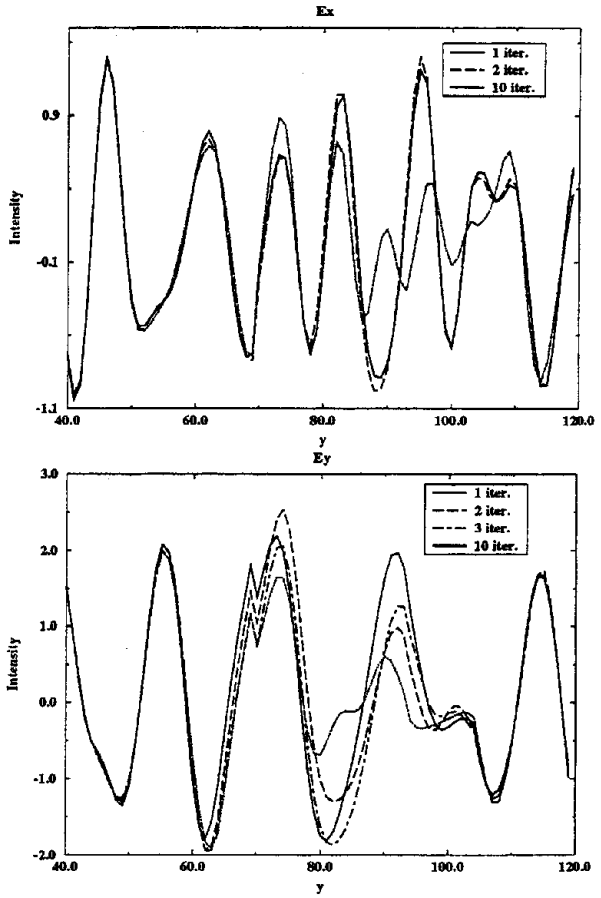

Figure 4: Components E_x (top) and E_y (bottom) at different iterations in the example shown in figure 2. The spatial coordinate along the dashed line is reported on the x axis

Provided that T is negligible, we have:

$$e^{ikr} = e^{ikr_0}\, e^{-i\mathbf{k}\cdot(\mathbf{x}' - \mathbf{x}'')} \qquad (7)$$

Let d' and d'' be the diameters of the regions S_1 and S_2. To get a quantitative estimate, we impose that the error on the phase is bounded by $\frac{\pi}{8}$. Then, looking at equation (6), we can see that T is negligible when

$$\frac{(d' + d'')^2}{8r_0} < \frac{\lambda}{16} \implies (d' + d'') < \sqrt{\frac{\lambda r_0}{2}} \qquad (8)$$

which is equivalent to the well-known far field relation. In this approximation, equation (4) becomes:

$$\mathbf{E}_s(\mathbf{x}) = \frac{i}{4\pi}\frac{e^{ikr_0}}{r_0}\, e^{i\mathbf{k}\cdot\mathbf{x}''}\mathbf{F}(\mathbf{k}) \qquad (9)$$

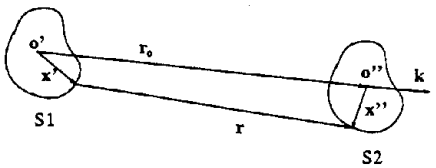

Figure 5: Scattering geometry

$$\mathbf{F}(\mathbf{k}) = \oint_{S_1} e^{-i\mathbf{k}\cdot\mathbf{x}'} \{k(\mathbf{n}' \times \mathbf{B}_s) + [\mathbf{k} \times (\mathbf{n}' \times \mathbf{E}_s) - \mathbf{k}(\mathbf{n}' \cdot \mathbf{E}_s)] \left(1 + \frac{i}{kr}\right)\} dx' \qquad (10)$$

In equation (10), the integral does not depend on the coordinate $\mathbf{x}''$ internal to the region S_2. Therefore, when we decompose the surfaces into regions which are small compared to their relative distance, we need to evaluate the integral only once for each region.
Since the area of the surface regions is proportional to r_0 (see equation (8)), with this approximation the computational time for the evaluation of the interaction between two surfaces is inversely proportional to their relative distance r_0. Moreover, the probability that one building A_1 "can see another building" A_2 (i.e. there aren't buildings between A_1 and A_2) decreases exponentially with r_0. Then, it can be demonstrated that the computational time grows as $N^{\frac{3}{2}}$ with the number N of transparent buildings and linearly with the number of opaque ones.

In order to check these results, we have performed some computations on configurations of n^2 buildings with $n = 2, \ldots, 6$ illuminated by the field emitted from an antenna. The buildings have been uniformly distributed over a square region (n per direction) and the antenna has been located at the center of the layout. The results are shown in figure 6 where $N = n^2$ represents the number of buildings and the relative computational time is defined as the ratio T_N/T_4 between the computational time required for N buildings and that required for 4 buildings. We can see that the scaling of time is similar to $N^{\frac{3}{2}}$ for a small number of buildings and to N further.

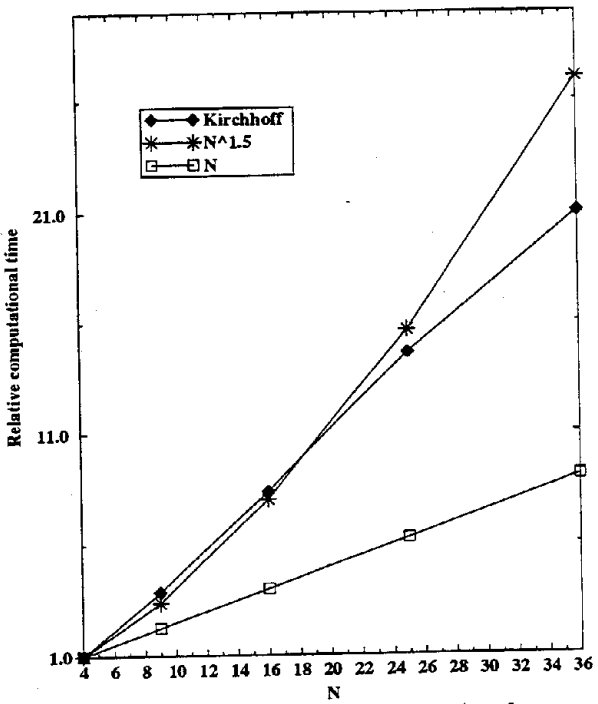

Figure 6: Scaling of the relative time T_N/T_4 for a regular distribution of $\sqrt{N} \times \sqrt{N}$ buildings. Black diamonds correspond to times measured for the Kirchhoff integral method

4.2 Reflections on the ground

In the simulation of the radioelectric propagation in urban areas, a numerical treatment of the ground using the Kirchhoff integral is, from a computational point of view, expensive.

We assume therefore that the reflection from the ground can be computed by Geometrical Optics. This assumption cannot be done for reflection from the buildings' walls. We refer to figure 7 for a brief explanation. The effects of diffraction, which are neglected by GO, are noticeable only near the light-shadow boundaries of the incident and reflected field. These boundaries exist only when we deal with reflections from the wall. For ground reflections, the incident and reflected fields have no discontinuities.

For the ground-wall double reflection, the discontinuity is inside the domain (see figure 8), but is partially compensated by the discontinuity due to the wall-ground double reflection. Since the wall and the ground form a 90 degree angle, the two discontinuities coincide, and it can be seen that the values of the two contributions are similar.

We notice that in the case of perfectly conducting walls and ground, the effects of diffraction are nonexistent. In fact the two surfaces give only three distinct contributions, two corresponding to single reflections on the walls, one corresponding to a double reflection. Each contribution can be attributed to a different image source and is accounted for by GO.

In figure 9, points A and B represent a source and a receiver respectively. The source can be either the antenna or any point of a scattering surface while the receiver can be either any point of a different scattering

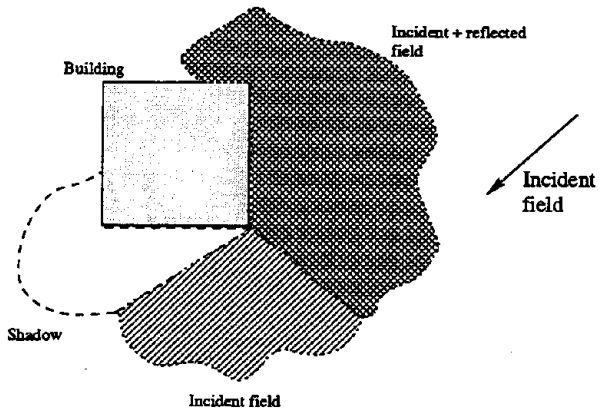

Figure 7: Light-shadow boundaries of the incident and reflected field

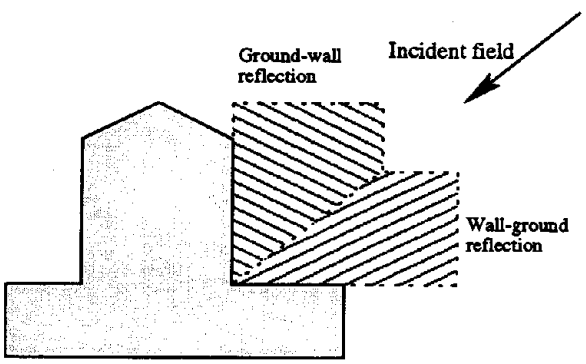

Figure 8: Geometrical description of the ground-wall double reflection paths

surface or any point where we want to compute the field value.

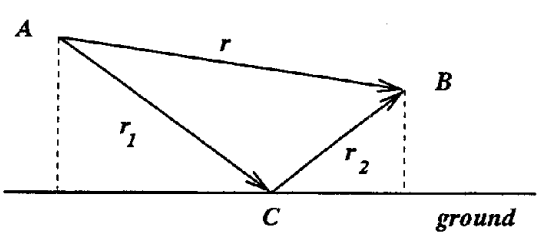

Figure 9: Geometrical scheme to illustrate ground reflections treatment

For each direct path **r** from A to B, there is another path $\mathbf{r}_1$ and $\mathbf{r}_2$ which involves one reflection on the ground at the point C. The contribution of the reflection in C to the field value in B is computed considering the lengths r_1, r_2 and by using Fresnel coefficients.

These considerations have been validated by implementing both the explicit (evaluation of the Kirchhoff integral) and implicit (Geometrical Optics) treatments of reflections on the ground and comparing the results on a test configuration. The layout (position of buildings and observation axis) is schematically described in figure 2. The input data of the simulation are equal to those given in section 3, with $\epsilon = 4$. The implicit treatment of ground reflections brings to numerical results which are similar to those obtained with an explicit one (see figure 10) and it allows, at the same time, a sensible reduction in both the computational time and storage memory. Moreover, it avoids the generation at the ground boundary, of fictitious diffraction terms which decrease the computed field when ground reflections are explicitly considered.

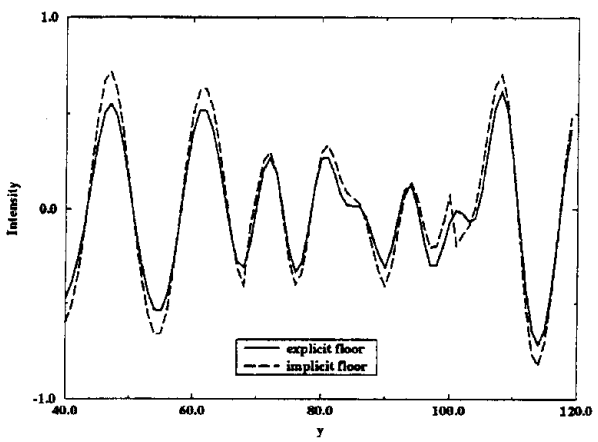

Figure 10: Component E_x of the electromagnetic field. The continuous line represents the field obtained by explicitly computing ground reflections with the Kirchhoff integral; the dashed line represents the field obtained by implicit (purely GO) ground treatment

5 Results

In sections 3 and 4, we have presented some results related to the convergence and time complexity of the method described here. The validation of the approach described in this paper is done by comparing the simulation outcome with a number of experimental measurements. In this section, we are going to present the results of these comparisons.

5.1 Radioelectric coverage in an urban environment

We give here the results of a numerical simulation of the propagation of the field emitted by an antenna throughout an urban environment. In figure 11, the white blocks represent the buildings of a real city and their parameters

(dielectric constant ϵ, height h_b, etc.) have been chosen uniformly over the layout because of the lack of detailed measurements. In particular, we have chosen $\epsilon = 4$ and $h_b = 10$ meters. The frequency of the field emitted by the source (antenna with a nonisotropic radiation pattern) is 1.8 GHz which corresponds to a wavelength of 16.7 centimeters. Input power is 250 mW. The source is located at a height of 4.5 meters and the electric field is computed at a height of 1.6 meters.

The cross in the center of the figure marks the position of the source and the gray scale indicates the simulated field power, decreasing from white to black. For an area of about 300 meters diameter, the whole simulation has taken 24 hours on a RISC/6000 560 IBM.

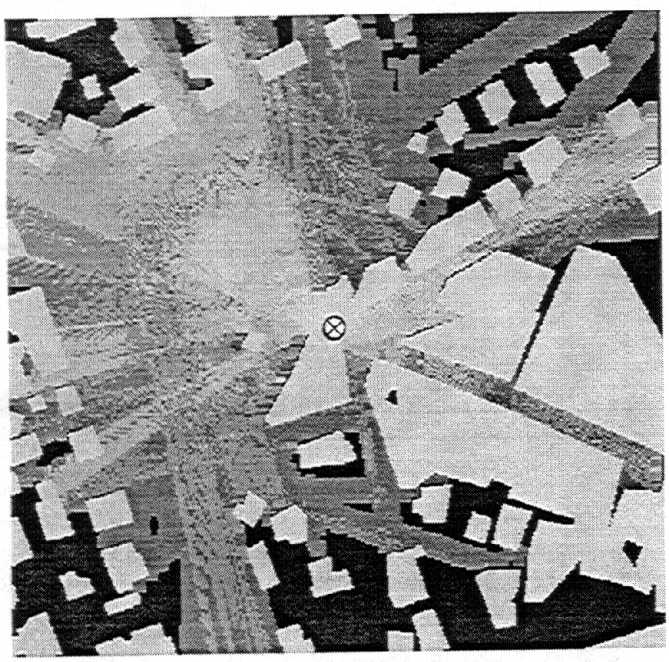

Figure 11: Example of the power emitted by an anisotropic antenna, obtained by the Kirchhoff integral method.

5.2 Comparison with experimental measurements

Comparisons with experimental measurements in realistic conditions are quite difficult because of the absence of accurate data on the computational domain. The dielectric constant of the involved materials and the height of the buildings are not known. Moreover, the map of the town is available with a precision of one meter; therefore, the direction error for shorter walls can be of the order of about ten degrees which doubles when we consider the direction of the reflected field. Further, due to interference phenomena, the field can vary considerably within one meter. Finally, no information is available about the presence of objects other than buildings; a parked car can easily intercept the ground-reflected field.

In these conditions, the computed power may easily differ by 10 to 20 dbm from the measured one and point-to-point comparisons cannot be used to validate or invalidate the code. On the other hand, the errors are fairly localized and the code can be still used with some confidence to estimate the coverage areas.

In the following figures, the cross marks the position of the antenna, while the numbered dots indicate the positions of the points where measurements have been taken. The light gray defines the area where the computed power is above threshold for both Geometrical Optics and Kirchhoff's method. The dark gray indicates the area where the power values are above threshold only for Kirchhoff's method. The area where the computed power values are below threshold is represented in black. The input data for both simulations (buildings' parameters, source's frequency, area's diameter) are equal to those used in section 5.1. Experimental data were obtained by a DECT system using propagation tester Symbionics SP935.

In figure 12, the computed coverage area of the antenna is represented for a threshold power of -85 dbm. It can be seen that the coverage area evaluated with Geometrical Optics is about 20% less than obtained with Kirchhoff's method. Moreover, two of the points considered ($\{5, 7\}$) lie outside it, while all the measured values and those evaluated with Kirchhoff's method are above threshold. Figure 13 has been obtained by raising the threshold up to -70 dbm. The measured values fall under the threshold in four points $\{1, 2, 3, 4\}$ and three of them are outside or very close to the boundaries of Kirchhoff's coverage area. The only evident discrepancy concerns point $\{4\}$ whose measured value is under the threshold while both Geometrical Optics and Kirchhoff's calculations locate it inside the illuminated region. Therefore, on the one hand, Kirchhoff's estimate of the coverage area clearly improves the Geometrical Optics one; on the other hand, due to the inaccuracy of the input data, the reliability of the results is limited and it is advisable to use a fairly large margin of safety.

6 Conclusions

The starting point for the planning and maintenance of any mobile communication network is based on a prediction of the radio wave attenuation around the source (antenna) in the layout of the buildings. In this paper we have proposed an iterative procedure based on the Kirchhoff integral method. Results have shown that this method is well suited to solve this problem and offers promising prospects of development in this field. The

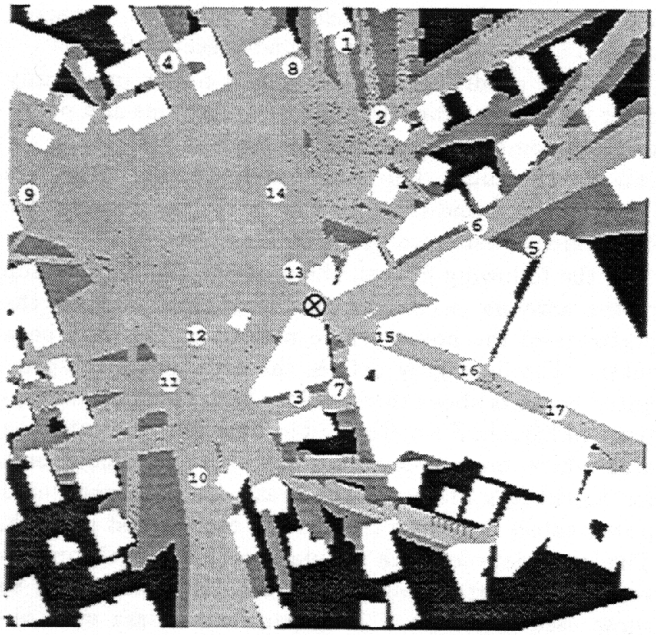

Figure 12: The coverage region of the antenna for a threshold power of -85 dbm. The light gray area defines the zone where both Geometrical Optics and Kirchhoff's method predict a value for the field power above threshold. The dark gray area corresponds to the zone where only the value predicted by Kirchhoff's method is above threshold. The black area defines the zone where both Geometrical Optics and Kirchhoff's method predict values below threshold. The antenna location is indicated by the cross, while the numbered dots indicate the location of receivers for experimental measurements

Figure 13: The coverage region of the antenna for a threshold power of -70 dbm. The meaning of the symbols and grey scale is the same as figure 12

model is currently under revision to improve its time requirements (Pisani, 1997).

7 Acknowledgements

We would like to thank Prof. G. Mazzarella of the University of Cagliari for helpful discussions and comments on the manuscript. We acknowledge A. Loche for providing us with a graphic interface for the visualization of the radioelectric coverage and Ing. F. Tallone of the Centro Studi e Laboratori Telecomunicazioni (CSELT) of Turin for providing us with experimental measurements. This work has been carried out with the financial support of Telecom Italia and the Sardinia Region Authorities.

References

- F. Ikegami, T. Takeuchi, and S. Yoshida, "Theoretical prediction of mean field strength for urban mobile radio", **IEEE Trans. Antenn. Propagat.**, vol. 39, pp. 299-302, 1991.
- J. D. Jackson, **Classical Electrodynamics**, John Wiley & Sons, New York (1975).
- T. Kürner, D.J. Cichon, and W. Wiesbeck, "Concepts and results for 3D digital terrain-based wave propagation models: an overview", **IEEE J. Select. Areas Commun.**, vol. 11, no. 7, pp. 1002-12, 1993.
- P. O. Luthi, B. Chopard, J-F Wagen, " Wave Propagation in Urban Microcells: a Massively Parallel Approach Using the TML Method", **Lecture Notes in Computer Science**, vol. 1041, pp. 408, 1996.
- L. Pisani, " Dimensionality reduction in the numerical evaluation of electro-magnetic scattering: from the Kirchhoff's integral method to a zero dimensional approach", submitted to **Computer Phys. Commun.**.
- K. Rizk, J-F Wagen, F. Gardiol, " Ray tracing based path loss prediction in two microcellular environments", in **Proceedings IEEE PIMRC'94**, pp. 210-4, The Hague, Netherlands, 1994.
- J.P. Rossi, A.J. Levy, "A ray model for decimetric radiowave propagation in an urban area", **Radio Science**, vol. 27, no. 6, pp. 971-9, 1992.